Modelling of cutting force and surface roughness of ultrasonic-assisted drilling using artificial neural network

Abdallah Abdelkawy*

*Correspondence:
abdallah.abdelkawy@ejust.
edu.eg

Mechanical Design
and Production Engineering
Department, Faculty
of Engineering, Cairo University,
Giza, Egypt

Abstract

This paper presents artificial neural network modelling for the thrust force in terms of maximum and mean values and the surface roughness for drilling soda glass using ultrasonic-assisted drilling. The experimental parameters are the tool concentrations (normal and high), cutting speed, and feed rate. The feedforward architecture neural network is composed of 10 hidden layers with sigmoid function and output layer with linear function. Three models are developed for each response individually and then one model for the three outputs. The models between the neural network output and the target (experimental results) for training, validation, and test data are developed, and their coefficients of regression are reasonable for this experimental data. The suitable number of hidden layers is examined with mean square error, and it is found that it decreases with increasing the number of hidden layer. The three models are developed based on one output, and the model of the three outputs is very close and good representative for the experimental results. It is concluded that the variables can be controlled and optimized by the same conditions.

Keywords: Neural network, Ultrasonic-assisted drilling, Feedforward, Soda glass, Thrust force

Introduction

Artificial neural network (ANN) is defined as a computational modelling method for experimental data based on input conditions. ANN simulates the human brain working. ANN is composed of inputs, artificial neurons of elements with different weights [1]. The importance of ANN comes from its ability to use nonlinear models, high capability to learn with high speed, and no assumptions are needed as in the case of analytical modelling. ANN performance can be improved by adding experimental data [2]. The artificial neural network is a successful prediction method for machinability measures such as cutting forces, surface roughness, and material removal rate [3–5]. In this regard, S. Sada [6] used ANN to predict the material removal rate and the surface roughness for mild steel turning. His model was based on the feedforward network. He concluded that the Levenberg–Marquardt (LM) and scaled conjugate gradient (SCG) training algorithms are convenient for predicting model for turning. N. Nagaraj et al.

[7] carried ANN model for surface roughness, and material removal rate was measured during grooving assisted with hot air for soda glass workpieces. Their model properties were learngdm for learning function, mean square error (MSE) for performance function, and 10 hidden neurons.

Ultrasonic-assisted drilling (UAD) is recommended for most brittle materials such as glass, carbon fiber-reinforced plastics, and metal matrix composites. UAD process is a hybrid of the ultrasonic machining and drilling. The process parameters are the cutting speed, feed rate, abrasive tool concentration, frequency, and amplitude. The experimental outputs can be the thrust force, surface roughness, edge chipping, and geometrical aspects [8–10]. The main force resulting during UAD is the thrust force in z-axis due to the ultrasonic vibration and feed rate. The thrust force is required to predict the cracks behavior, the edge chipping, and the surface roughness. In this regard, the high thrust force increases with the feed rate increase and the decrease of spindle speed [9, 11, 12]. Moreover, the lower thrust force reduces the hole edge tearing size [13]. Wu et al. [14] measured mean and maximum thrust force during their experiments of alumina UAD and found that they decreased at high spindle speed and low feed rate. Ning et al. [15] found similar trends when carried out carbon fiber-reinforced plastic drilling and stated that the reason for this trend is the lower contact time between the abrasive tool and the workpiece in UAD. The intermitted contact in UAD [16] and the reduction of the friction due to the increasing the cutting speed [17] are the main reasons for the reduction in the thrust force.

Modelling the thrust force and surface roughness for UAD is an important objective for reducing the experiments by predicting them for further conditions and finding optimum conditions [18–20]. J. M. Baraheni et al. developed statistical model for UAD of composite of LY160/HA-11/T700. They found that the low feed rate and high spindle speed had a significant effect on reduction of the thrust force hence reduction of the fibers delamination [21]. Many mathematically based process physics models were developed. Pei et al. [22] proposed that the shape of the removed chips is an ellipsoid. Liu et al. [23] assumed the abrasives were in the shape of octahedron and the fracture zone was in tetrahedron shape. Although there are many trials of mathematical and statistical modelling of thrust force of UAD, there is no trails to used artificial neural network.

Surface roughness also is a crucial output for machining processes because it judges the level of the machined part finish. N. Guba et al. [24] found that the UAD improved the hole surface finish compared to the conventional drilling. Generally, The higher spindle speed and the lower feed rate reduced the surface roughness (Ra) as found in many previous studies [25–27]. Zhang et al. [9] tested UAD of K9 glass and found that Ra increased marginally in case of higher vibration amplitude. Moreover, high feed rate and low spindle speed deteriorated the surface quality. Jiao et al. [28] developed statistical model for the surface roughness during UAD of alumina and found that the feed rate was the significant factor. Moreover, surface roughness (Ra) decreased with spindle speed, increase of grit size, and decrease of feed rate. J. Airao et al. [29] investigated the effect of different cooling strategies on the surface roughness during ultrasonic-assisted turning. They found that using minimum quantity lubrication (MQL) and CO_2 reduced the surface roughness greatly compared to dry cutting.

The main objective of this paper is using the artificial neural network to model the machinability variables: maximum and mean thrust force and the surface roughness measured by Ra. The models are developed to monitor the effect of the tool concentration, cutting speed and feed rate on thrust force, and surface roughness to continuously adjust the cutting conditions to maintain these outputs within the acceptable ranges. Four models are developed: one model for each variable separately, and the other model was developed based on the three variables. A comparison was held between the output of the models of single variable and the output of the multivariable to find the capability of the multivariable model to express the variables. Some of these experimental results without artificial neural network modelling were published before in these references [8, 30, 31].

Development of neural network model

Experimental work related to ANN

The experimental work related to this study involved measuring the mean and maximum thrust force and surface roughness for UAD. The used material as workpiece was soda glass due to their importance in biomedical and chemical applications. The workpiece material chemical composition is SiO_2 (69–74%), Na_2O (10–16%), and CaO (5–14%). The experiments were carried out using the DMG-MORI ULTRASONIC 20. Linear maximum rotational speeds with and without ultrasonic vibration are 40,000 rpm and 42,000 rpm, respectively. The used cutting tools were electroplated diamond core drills (SCHOTT Ltd. Corp.) with outer diameter and wall thickness of 6 mm and 0.5 mm, respectively. Figure 1 shows the experimental setup.

The thrust force on the cutting tool was measured using Kistler dynamometer (force sensor) type 9272. The mean and maximum values of thrust force are taken in this study. The surface roughness was measured in terms of the arithmetical mean value (Ra) using the surface roughness tester TR-200. The ultrasonic vibration conditions were 28 kHz of frequency and 10 mμ of amplitude. The experimental parameters were the abrasive particles concentration of the cutting tool, the spindle speed, and the feed
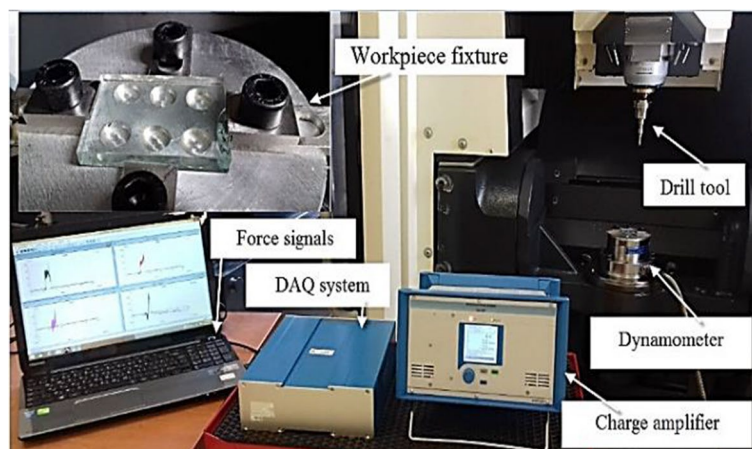

Fig. 1 Experimental setup

rate as shown in Table 1. The measured outputs for maximum and mean thrust force (N) and the surface roughness (μm) are shown in Table 2.

Artificial neural network model development

Four models are developed in this study: one model is developed for mean and maximum thrust force and the surface roughness Ra separately and then one model to predict the three responses directly. The model conditions are defined form the literature review. The feedforward architecture is selected in this study with multi-hidden layers with sigmoid functions (Eq. (1)) and one layer with linear function (Eq. (2)) before the output layer. Due to the sigmoid function range from 0 to 1, the experimental true results are normalized as shown in Table 2 [2, 32, 33]. Equation (3) was used to normalize the experimental data.

Many trials were carried out for defining suitable number of hidden layers. Figure 2 shows the mean squared error (MSE) for three runs for models for the maximum and mean thrust force and the surface roughness with the number of hidden layers. It is found that the MSE decreases with increasing the number of the hidden layers while increasing the number of hidden layer increases the time of model running. It is noticed that a large decrease for the MSE occurs at 10 hidden layers, and it is suitable for the running time. The percentages of training, validation, and testing data were taken from similar publish work [32, 34]. They are selected to be 70%, 15%, and 15%, respectively. The most selected training function is Levenberg–Marquardt as most of similar problems [6, 34, 35]. The mean squared error is used to measure the models performance. Matlab R2020b-academic was used to carry out the model runs.

$$Y = \frac{1}{1 + \exp(-x)} \tag{1}$$

$$Y = ax + b \tag{2}$$

$$x_i = \frac{d_i - d_{min}}{d_{max} - d_{min}} \tag{3}$$

where x_i is the normalized data corresponding to the experimental data (d_i). The symbols d_{min} and d_{max} are the minimum and maximum experimental data values.

Table 1 Experimental levels of the selected parameters

Factors	Levels				
	1	2	3	4	5
Tool concentration	High (*H*) (100%)	Normal (*N*) (50%)			
Spindle speed (rpm)	3000	5000	7000	8000	
Feed rate (mm/min)	0.6	2.4	3.3	4.2	6

Table 2 The actual and normalized experimental results of the thrust force (maximum and mean) and the surface roughness

No	True values						Normalized values					
	Tool con	Speed (rpm)	Feed (mm/min)	FZ mean (N)	Fz max (N)	Ra (μm)	Tool con	Speed (rpm)	Feed (mm/min)	FZ mean (N)	Fz max (N)	Ra (μm)
1	H	3000	0.6	10.37	38.55	0.64	0	0	0	0.48	0.68	0.02
2	H	3000	2.4	16	31.34	0.68	0	0	0.34	0.75	0.45	0.07
3	H	3000	3.3	15.44	25.67	0.87	0	0	0.5	0.72	0.26	0.36
4	H	3000	4.2	17.54	27.34	1.07	0	0	0.67	0.82	0.31	0.65
5	H	3000	6	18.54	27.94	1.17	0	0	1	0.87	0.33	0.81
6	H	5000	0.6	4.8	36	1.08	0	0.4	0	0.21	0.6	0.67
7	H	5000	2.4	11.69	28.67	0.99	0	0.4	0.34	0.54	0.36	0.54
8	H	5000	3.3	15.8	25.2	1.03	0	0.4	0.5	0.74	0.24	0.59
9	H	5000	4.2	12.84	21.87	1.23	0	0.4	0.67	0.6	0.13	0.89
10	H	5000	6	17.57	25.67	1.07	0	0.4	1	0.82	0.26	0.66
11	H	7000	0.6	6.34	44.67	0.64	0	0.8	0	0.29	0.89	0.01
12	H	7000	2.4	10.37	24	0.98	0	0.8	0.34	0.48	0.2	0.53
13	H	7000	3.3	13.17	23.34	0.98	0	0.8	0.5	0.61	0.18	0.52
14	H	7000	4.2	17.15	27.67	0.93	0	0.8	0.67	0.8	0.33	0.45
15	H	7000	6	14.64	23.1	1.04	0	0.8	1	0.68	0.18	0.62
16	H	8000	0.6	2.83	37.34	1	0	1	0	0.12	0.64	0.55
17	H	8000	2.4	10.88	27	1.14	0	1	0.34	0.5	0.3	0.75
18	H	8000	3.3	16.17	28.67	0.87	0	1	0.5	0.76	0.36	0.35
19	H	8000	4.2	15.67	27.92	0.92	0	1	0.67	0.73	0.33	0.44
20	H	8000	6	17.54	26.57	0.96	0	1	1	0.82	0.29	0.49
21	N	3000	0.6	11.04	40.34	0.91	1	0	0	0.51	0.74	0.42
22	N	3000	2.4	18.67	27	0.96	1	0	0.34	0.88	0.3	0.5
23	N	3000	3.3	17.87	28.2	1.02	1	0	0.5	0.84	0.34	0.58
24	N	3000	4.2	21.34	27.27	1.27	1	0	0.67	1.01	0.31	0.95

Table 2 (continued)

| No	True values							Normalized values					
	Tool con	Speed (rpm)	Feed (mm/min)	FZ mean (N)	Fz max (N)	Ra (μm)		Tool con	Speed (rpm)	Feed (mm/min)	FZ mean (N)	Fz max (N)	Ra (μm)
25	N	3000	6	18.87	27.24	1.08		1	0	1	0.89	0.31	0.67
26	N	5000	0.6	7.96	38	0.77		1	0.4	0	0.36	0.67	0.21
27	N	5000	2.4	19.51	31.34	0.83		1	0.4	0.34	0.92	0.45	0.29
28	N	5000	3.3	16.27	24.2	1.01		1	0.4	0.5	0.76	0.21	0.56
29	N	5000	4.2	17.67	24.67	1.01		1	0.4	0.67	0.83	0.23	0.56
30	N	5000	6	14.69	22.07	1.07		1	0.4	1	0.69	0.14	0.65
31	N	7000	0.6	3.26	36.34	0.77		1	0.8	0	0.14	0.61	0.21
32	N	7000	2.4	12.53	24.5	0.97		1	0.8	0.34	0.58	0.22	0.5
33	N	7000	3.3	11.3	21.84	1.08		1	0.8	0.5	0.53	0.13	0.67
34	N	7000	4.2	17.2	23.67	1.12		1	0.8	0.67	0.81	0.19	0.72
35	N	7000	6	18.24	25.34	1.32		1	0.8	1	0.86	0.25	1.03
36	N	8000	0.6	5.78	48.34	0.73		1	1	0	0.26	1.01	0.15
37	N	8000	2.4	13.34	24.54	0.77		1	1	0.34	0.62	0.22	0.21
38	N	8000	3.3	19.79	28.87	0.87		1	1	0.5	0.93	0.37	0.35
39	N	8000	4.2	12.61	20.74	0.79		1	1	0.67	0.59	0.1	0.23
40	N	8000	6	16.67	23	1.14		1	1	1	0.78	0.17	0.76
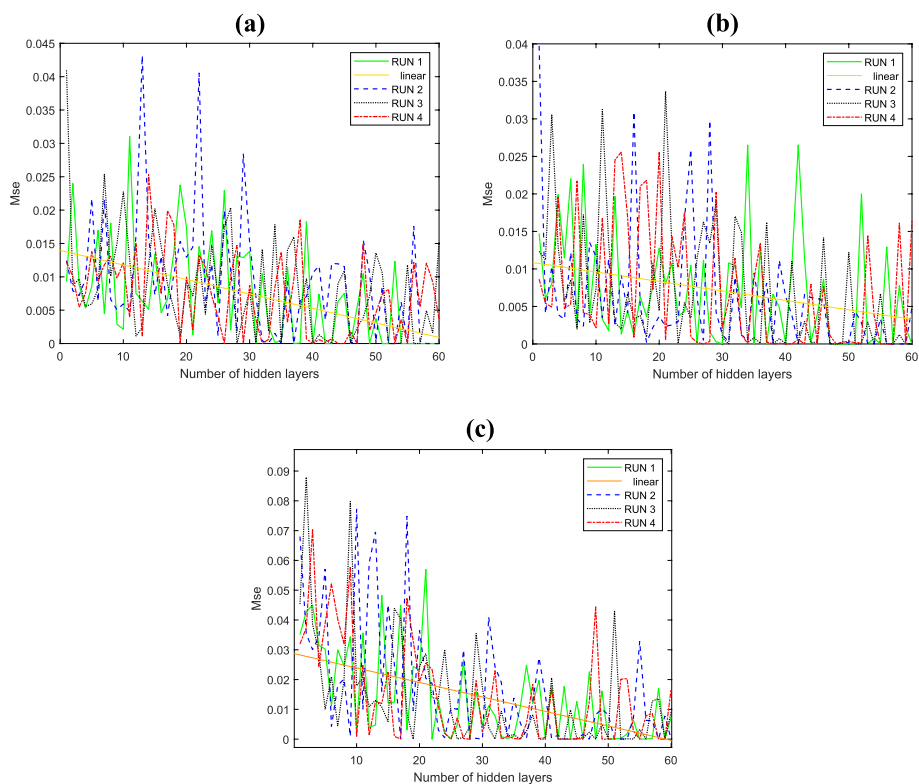
Fig. 2 The effect of the number of hidden layers on the mean squared error for results of **a** mean thrust force, **b** maximum thrust force, and **c** surface roughness Ra
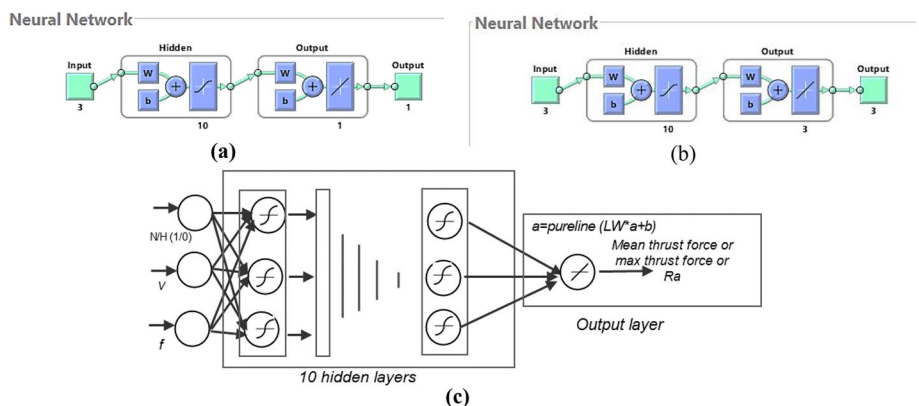

Fig. 3 The neural network architecture for **a** one output model and **b** three outputs models and **c** detailed used of neural network architecture

Results and discussion

Figure 3a shows the ANN architecture which is used to predict only output (mean or maximum thrust force or surface roughness), and Fig. 3b shows the architecture was used to model the three outputs at the same time. Figure 3c shows the detailed architecture developed. Table 3 shows the neuron weights and biases for all layers. During ANN

Table 3 The neurons weights and biases for the neural network for the mean and maximum thrust force and surface roughness

Layer	FZ mean				Fz max				Ra				All			
	W1	W2	W3	b	W1	W2	W2	b	W1	W2	W3	b	W1	W2	W3	b
1	− 0.2	1.5	− 2.7	3	2.9	0.9	0.4	− 2.9	− 2.7	− 0.1	1.4	2.9	3	− 0.6	0.5	− 2.8
2	− 1.1	− 1.7	2.2	2.3	3.3	− 0.1	1.5	− 1.8	− 2.1	1.7	− 2	2.7	1.8	1.6	− 0.8	− 2.5
3	− 1.6	− 1.6	− 2.3	1.4	− 0.3	− 3.3	− 0.6	2.3	− 1.9	0.4	2.7	2.6	− 3	− 1	− 0.1	1.6
4	2.8	0.2	− 1.1	− 1	1.7	− 2	1.3	− 0.7	− 1.6	− 2.7	0.6	1.5	1.5	− 2.5	0.5	− 1.1
5	− 1.8	0.3	− 1.9	0.3	0.4	− 2.1	− 2.3	0.1	− 1.4	2.2	− 1.3	0.5	2.1	0.4	2.2	− 0.4
6	1.8	− 0.3	2.7	0	2.3	− 0.7	− 2	0.8	− 1.4	− 2.6	0.7	− 0.2	1.9	− 1	− 2.6	1.1
7	− 1.8	− 1.2	1.3	− 0.9	2.8	0.8	0.8	1	− 2.6	1.8	2.6	− 1.6	2.7	− 0.3	0.9	1.1
8	1.2	− 1	2	2.2	− 2.7	1.6	0.5	− 1.8	1.4	− 2.5	0.8	1.5	0.3	− 0.5	2.9	1.9
9	0.8	− 2.8	1.4	2.1	− 0.1	1.1	− 3.2	2.4	2.6	− 1.2	− 0.5	2.4	1	− 1.8	− 2.6	2.1
10	1.5	− 0.4	− 2.6	3	− 1.4	1.9	1.2	− 3.4	− 1.1	3.8	− 0.7	− 2.3	− 3.1	− 0.2	0.2	− 3
Output				− 0.1				− 0.5				0.6				0.5
																− 0.1
																− 0.2

working, the neuron weights are arranged in matrix corresponding to the terms of (w) in Eq. 4 where each raw represents a layer, where $w_{1,1}$, $w_{2,1}$, $w_{1,2}$, and $w_{2,2}$ equal to -0.2, 1.5, -1.1, and -1.7, and so on. The dot product of each weight (w) column with the input vector then is summed to the corresponding bias (b) and then (x) in Eq. 4 is compensated in Eq. (1).

$$x = wp + b = \begin{bmatrix} w_{1,1} & w_{2,1} & w_{3,1} \\ w_{1,2} & w_{2,2} & w_{3,2} \\ . & . & . \\ . & . & . \\ w_{1,10} & w_{1,10} & w_{1,10} \end{bmatrix} \begin{bmatrix} N/H \\ v \\ f \end{bmatrix} + \begin{bmatrix} b1 \\ b2 \\ . \\ b10 \end{bmatrix} \tag{4}$$

The ANN model for the mean thrust force

Figure 4 shows the regression and performance plots for the developed model for the mean thrust force which is developed by neural nertwork technique. The regression plots (Fig. 4a) show that the artificial neural network model output is close to the experimental data. The regression coefficients (R^2) for the data used for training, validation, and test are 0.92, 0.93, and 0.93 respectively which are expressed in the high agreement of the model. When all data are fitted, the regression coefficient is 90%. The models of the true experimental data and the neural network output for training, validation, test, and the overall data are shown in Eq. 5, Eq. 6, Eq. 7, and Eq. 8, respectively. In Fig. 4b, the mean squared error decreased greatly for the training, validation, and test data with increasing the number of the training trials. The best performance for both validation and tested data at the third epoch about mean squared error (MSE) equals to 0.0296 and 0.009, respectively.

$$\text{Output}(\text{Fzmean} - \text{training}) = 0.83 \times \text{target} + 0.11 \tag{5}$$

$$\text{Output}(\text{Fzmean} - \text{validation}) = 0.54 \times \text{target} + 0.35 \tag{6}$$

$$\text{Output}(\text{Fzmean} - \text{test}) = 0.74 \times \text{target} + 0.13 \tag{7}$$

$$\text{Output}(\text{Fzmean} - \text{all}) = 0.72 \times \text{target} + 0.18 \tag{8}$$

The ANN model for maximum thrust force

The regression plots for fitting all experimental results of the maximum thrust force and the portions of data used for training, validation, and the test in addition to the performance plots are developed by neural nertwork technique as shown in Fig. 5a. The coefficients of regression (R^2) of the developed models show high representation for the experimental data especially in case of training ($R^2 = 96.6\%$), validation ($R^2 = 94.4$), and all data (94%), while test data is quite lower ($R = 86\%$). The equations correlate with the experimental results, and the output of the neural network for training, validation, and test data is Eq. 9, Eq. 10, and Eq. 11, respectively, and Eq. 12 correlates all results with ANN outputs. Figure 5b shows that the mean squred error decreases for the training, validation, and test data with training neural network model in many trails. The least MSE for validation data occurs at the trail 8 and in case of the tested data occurs at the sixth trail.
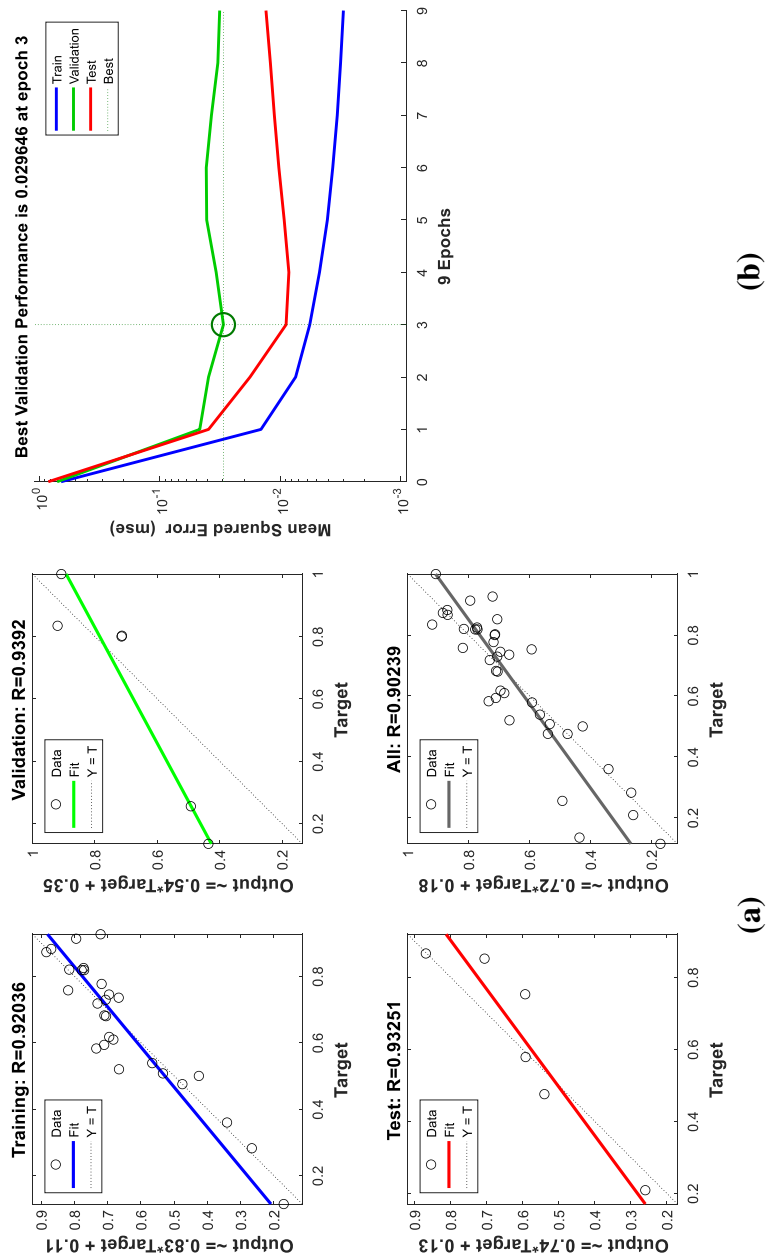
Fig. 4 Neural network outputs for the mean thrust force. **a** Regression plot and **b** performance plot
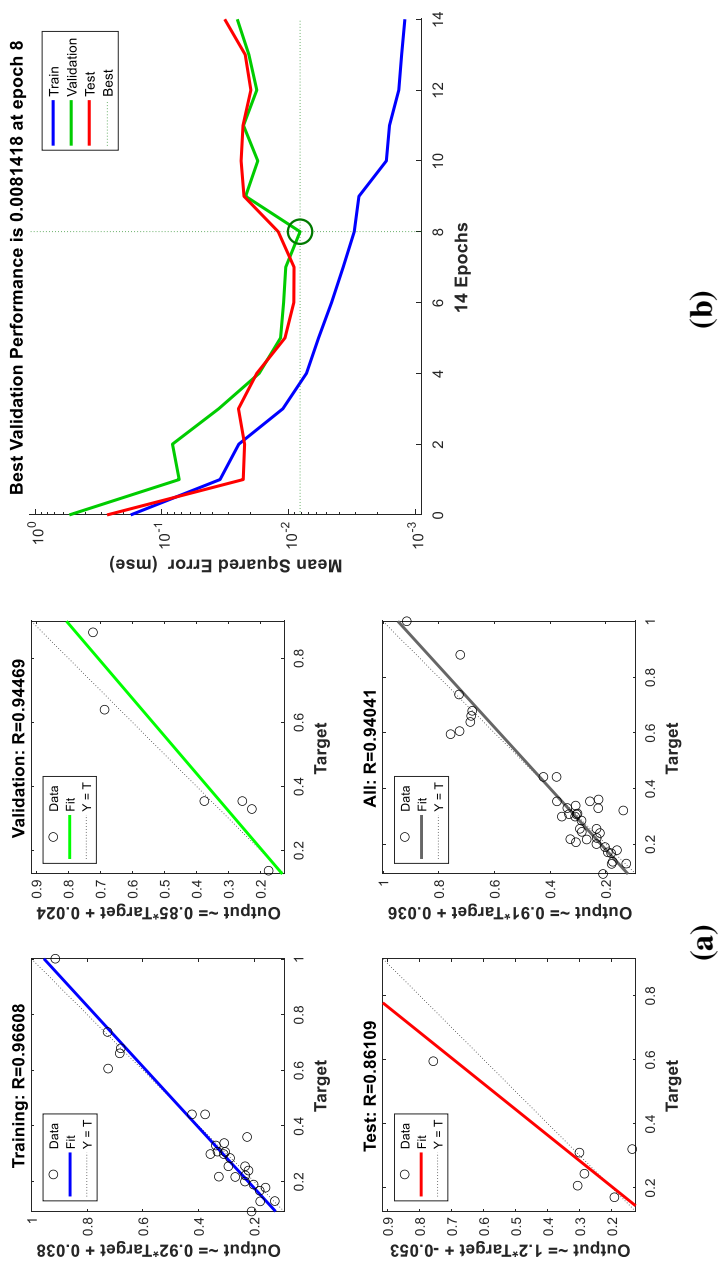
Fig. 5 Neural network outputs for the surface roughness Ra. **a** Regression plot and **b** performance plot

$$\text{Output}\big(\text{Fzmax} - \text{training}\big) = 0.92 \times \text{target} + 0.038 \tag{9}$$

$$\text{Output}(\text{Fzmax} - \text{validation}) = 0.85 \times \text{target} + 0.024 \tag{10}$$

$$\text{Output}(\text{Fzmax} - \text{test}) = 1.2 \times \text{target} + 0.053 \tag{11}$$

$$\text{Output}(\text{Fzmax} - \text{all}) = 0.91 \times \text{target} + 0.036 \tag{12}$$

The ANN model of surface roughness

The model with conditions is stated in section of development neural network model conditions with the normalized data of the surface roughness. Figure 6a shows the regression fitting of the true experimental results after dividing into training, validation, and test data in addition to the regression of all data. These models achieve higher coefficients of regression (R^2) for the surface roughness measurements (Ra) compared to the model of the mean thrust force. The coefficients of regression for training, validation, and test portions and all data are 95%, 95%, 91%, and 92%, respectively. Equations (12–15) are derived from the developed neural network to correlate to the true experimental results (target) and the output for training, validation, test, and all data. Figure 6b indicates that the mean squared error of the fitted values with the ANN trails decreases for the training, validation, and test data. The least MSE for validation data occurs at the fifth trail.

$$\text{Output}(\text{Ra} - \text{training}) = 0.89 \times \text{target} + 0.056 \tag{13}$$

$$\text{Output}(\text{Ra} - \text{validation}) = 1.3 \times \text{target} + 0.12 \tag{14}$$

$$\text{Output}(\text{Ra} - \text{test}) = 1.4 \times \text{target} + 0.28 \tag{15}$$

$$\text{Output}(\text{Ra} - \text{all}) = 0.99 \times \text{target} + 0.0091 \tag{16}$$

The ANN model for mean and maximum thrust force and surface roughness

This section concerns with the neural network model with the output of three machinability measures: the mean and maximum thrust force and the surface roughness Ra. This model is devolved for the manufacturing engineers for optimizing the three machinability measurements at the same conditions. It is developed with the same conditions of the previous models with the normalized data of the three experimental outputs. Figure 7a shows the regression of the fitted data of potions of the training, validation, and test data in addition to the regression of fitting all data. The coefficients of regression (R^2) for this model for training, validation, and test data are 94%, 85.8%, 83.4%, and 90%, respectively. They are a little low compared to the coefficient of regression of the previous models may be due to the variation of the three measurements, but it is important for the optimization of the three outputs at the same time. Equations (17–20) are developed from the neural network to correlate the true experimental results (target) and the output. Figure 7b indicates that
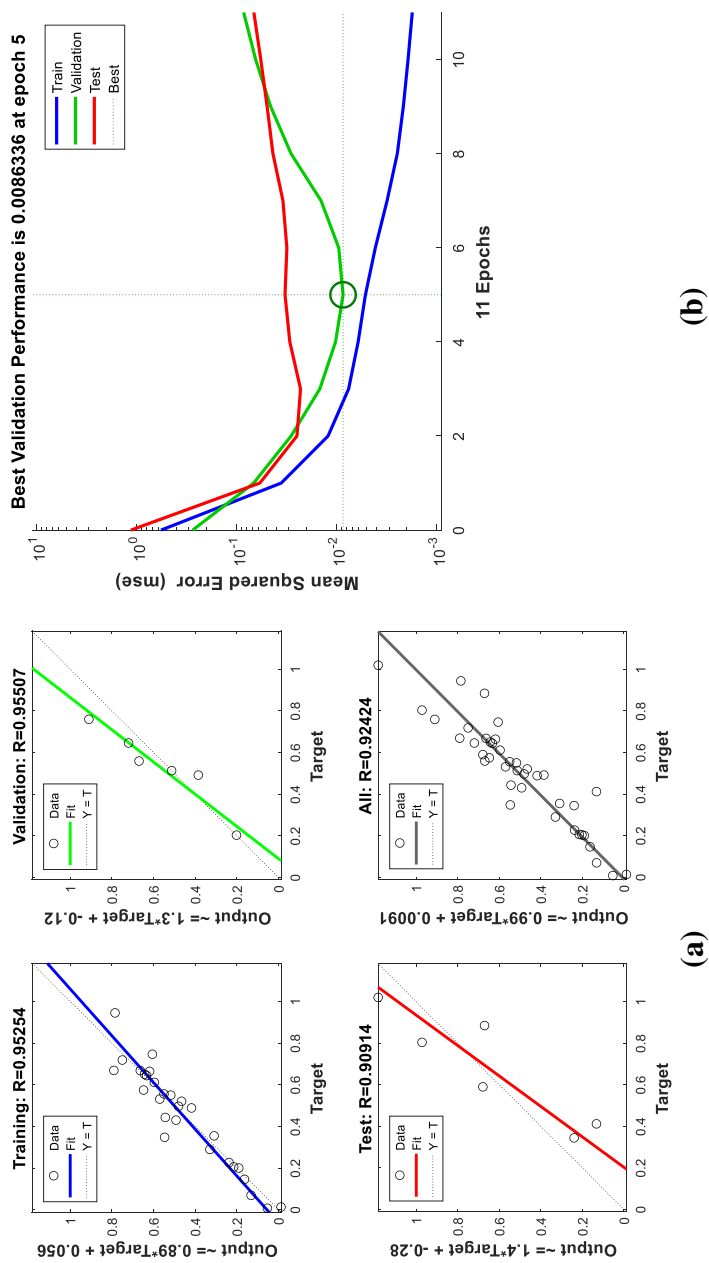
Fig. 6 Neural network outputs for the maximum thrust force (**a**), regression plot (**b**), and performance plot (**c**)
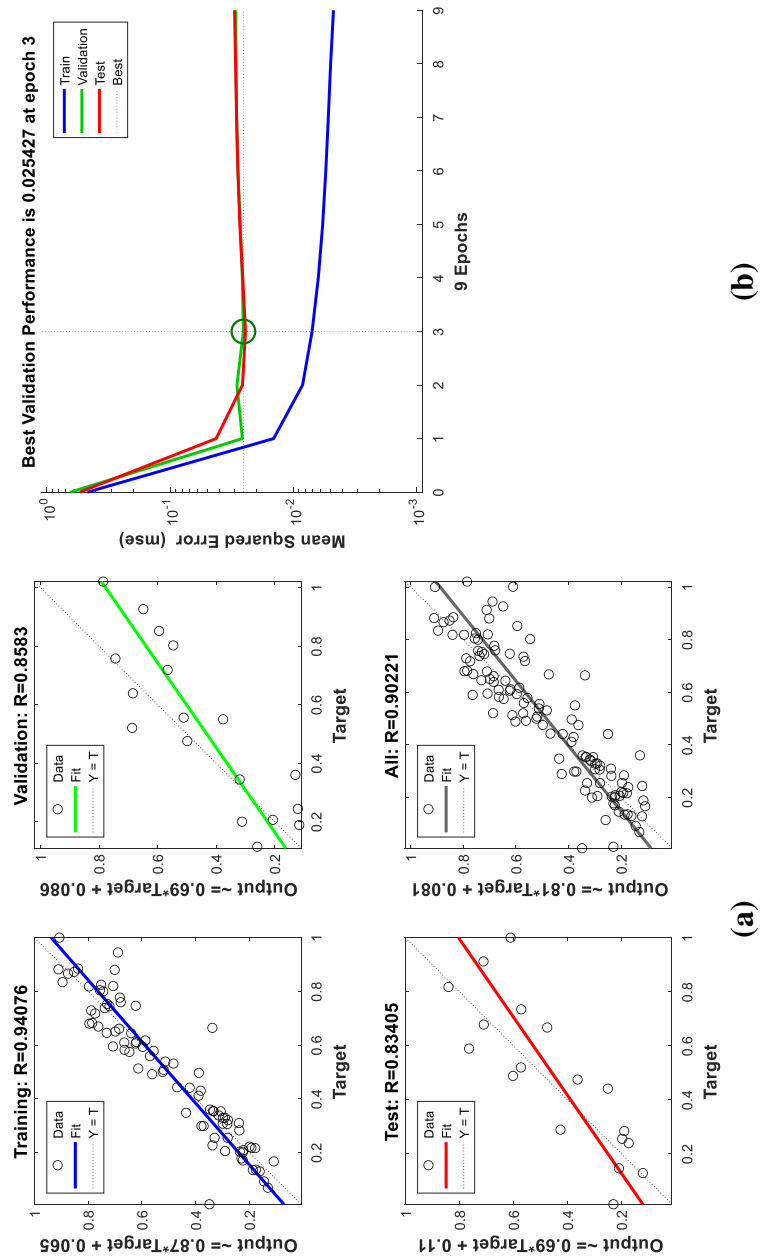
Fig. 7 Neural network outputs for the three meansured outputs. **a** Regression plot and **b** performance plot

the mean squared error of the fitted values with the ANN trail decreases for the training, validation, and test data. The least MSE for validation data occurs at the third trail.

$$\text{Output}(\text{training}) = 0.87 \times \text{target} + 0.065 \tag{17}$$

$$\text{Output}(\text{validation}) = 0.69 \times \text{target} + 0.086 \tag{18}$$

$$\text{Output}(\text{test}) = 0.69 \times \text{target} + 0.11 \tag{19}$$

$$\text{Output}(\text{all}) = 0.81 \times \text{target} + 0.081 \tag{20}$$

Figure 8 shows the comparison between the true experimental results, predicted output of the model developed for each machinability measurement separately and the output from the general model based on each measurement. The predicted outputs are developed based on Eqs. (5), (9), and (13) for the mean (Fz mean) and maximum (Fz max) thrust force and the surface roughness (Ra, respectively. Equation (17) is used to find the output for the three measurements. These equations are used because of their high coefficients regresion. Regarding Fig. 8a, the predicted outputs of the mean thrust force of the general model are closer to the real experimental data compared to the outputs of the model of the mean thrust force only. Figure 8b shows that the outputs of the model of the maximum thrust force are closer to the true experimental results compared to the general model. In case of the surface roughness Ra, the experimental results and the output of Ra model are nearly the same, while the general model produces an error in the range from 2.8 to 8.1% as shown in Fig. 8c. Generally, the models developed by the neural networks with the previous stated conditions are suitable representative for the experimental results. The errors between the experimental results and the predicted results from the models were calculated, and Table 4 summarizes the error range for each model predicted values compared to the experimental results.

Conclusions

The ANN models of mean and maximum thrust force and the surface roughness Ra of soda glass drilled using UAD are developed. The experimental conditions of tool concentration, feed rate, and spindle speed were modeled based on the experimental results using the neural network and using the feedforward architecture and 10 hidden layers. Three models were developed for each experimental variable individually based on one output model, and then, a three outputs model is developed for the three experimental outputs at the same time. The generated models give high coefficient of regressions. The general model controls the three outputs at the same time and saves the manufacturing engineers controlling for the inputs and lower thrust force and good surface roughness. The coefficients of regression for the developed model are quit high and suitable for these results. The following points conclude the paper outputs:

1. The artificial neural networks can be used to model machinability measures (mean and maximum thrust force and surface roughness) for ultrasonic-assisted drilling process with reasonable presentation for the experimental results.
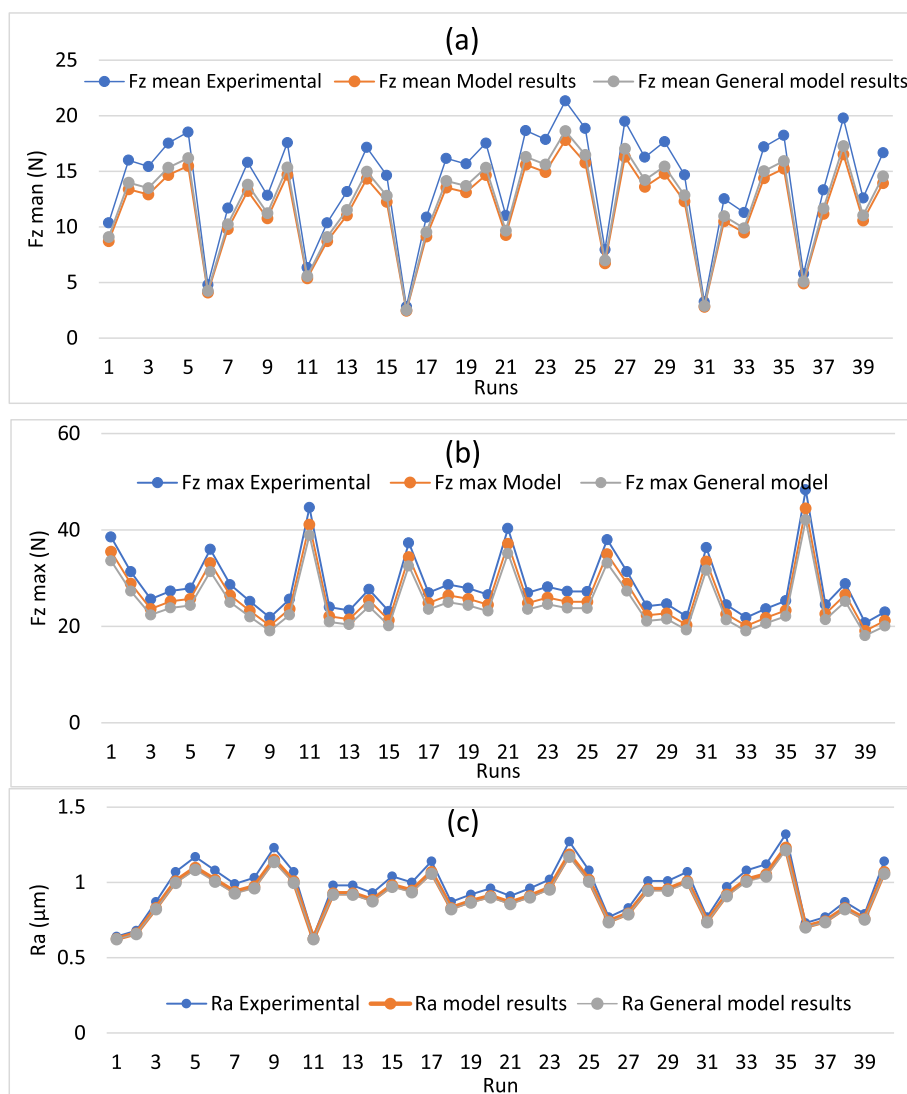
Fig. 8 Comparison between the experimental results, output of the model for each machinability measurement, and the output of the general model from the three measurements. **a** Mean thrust force (Fz mean), **b** maximum thrust force (Fz max), and surface roughness (Ra)

2. The three machinability measures can be modeled in one model to find optimum conditions for reducing the maximum and minimum thrust force and the surface roughness.

3. Generally, modelling each variable individually is more efficient in terms of coefficient of regression compared to one model for the three variables.

Table 4 The models error compared to the experimental results

Model output	Models of one output			Model of the three outputs		
	FZ mean (*N*)	Fz max (*N*)	Ra (*μm*)	FZ mean (*N*)	Fz max (*N*)	Ra (*μm*)
Max error	15	7.9	0.5	12.7	12.9	8.1
Min error	13	7.8	1	10	12.7	2.8

Abbreviations

ANN
Artificial neural
SCG
Scaled conjugate gradient
MSE
Mean square error
UAD
Ultrasonic-assisted drilling
x_i
Normalized data corresponding to the experimental data
Ra
Mean surface roughness
Fz
Thrust force
R^2
Regression coefficients
$d_i, d_{min},$ and d_{max}
Minimum and maximum experimental values

Declarations

Competing interests

The author declares no competing interests.

References

1. Agatonovic-Kustrin S, Beresford R (2000) Basic concepts of artificial neural network (ANN) modeling and its application in pharmaceutical research. J Pharm Biomed Anal 22:717–727
2. Mohd A, Haron H, Sharif S (2010) Prediction of surface roughness in the end milling machining using artificial neural network. Expert Syst Appl 37(2):1755–1768. https://doi.org/10.1016/j.eswa.2009.07.033
3. Lalwani V, Sharma P, Pruncu CI (2020) Response surface methodology and artificial neural network-based models for predicting performance of wire electrical discharge machining of Inconel 718 alloy. J Manuf Mater Process Artic 44(4):1–21
4. Manikandan N, Palanisamy D (2020) Optimisation of spark erosion machining process parameters using hybrid grey relational analysis and artificial neural network model Ramesh Raju. Int J Mach Mach Mater 22(1):1–23
5. Venkatesan D, Kannan K, Saravanan R (2009) A genetic algorithm-based artificial neural network model for the optimization of machining processes. Neural Comput Appl. 135–140. https://doi.org/10.1007/s00521-007-0166-y.
6. Sada SO (2021) Improving the predictive accuracy of artificial neural network (ANN) approach in a mild steel turning operation. Int J Adv Manuf Technol 112:2389–2398
7. Nagaraj Y, Jagannatha N, Sathisha N, Niranjana S J (2020) "Prediction of material removal rate and surface roughness in hot air assisted hybrid machining on soda-lime-silica glass using regression analysis and artificial neural network," Silicon
8. Abdelkawy A, Hossam M, El-hofy H (2019) Experimental investigation of surface and geometrical characteristics of rotary ultrasonic drilling of soda glass. Mach Sci Technol 23(3):385–406. https://doi.org/10.1080/10910344.2018.1486422
9. Zhang C, Cong W, Feng P, Pei Z (2013) Rotary ultrasonic machining of optical K9 glass using compressed air as coolant: a feasibility study. Proc Inst Mech Eng Part B J Eng Manuf. 228(4):504–514. https://doi.org/10.1177/0954405413506195.
10. Han Y, Lv Q, Song Y, Zhang Q (2022) "Influence of parameters on temperature rise and chips morphology in low-frequency vibration-assisted bone drilling." Med Eng Phys 103:103791. https://doi.org/10.1016/j.medengphy.2022.103791
11. Kumar V, Singh H (2019) Investigation of hole quality in rotary ultrasonic drilling of borosilicate glass using RSM. J Brazilian Soc Mech Sci Eng 41(1):1–16. https://doi.org/10.1007/s40430-018-1524-7
12. Anwar S, Nasr MM, Pervaiz S, Al-ahmari A, Alkahtani M, El-tamimi A (2018) A study on the effect of main process parameters of rotary ultrasonic machining for drilling BK7 glass. Adv Mech Eng 10(1):1–12. https://doi.org/10.1177/1687814017752212

13. Wang J, Feng P, Zheng J, Zhang J (2016) Improving hole exit quality in rotary ultrasonic machining of ceramic matrix composites using a compound step-taper drill. Ceram Int 42(12):13387–13394. https://doi.org/10.1016/j.ceramint.2016.05.095

14. Wu J, Cong W, Williams RE, Pei ZJ (2011) Dynamic process modeling for rotary ultrasonic machining of alumina. J Manuf Sci Eng 133(4):041012. https://doi.org/10.1115/1.4004688

15. Ning FD, Cong WL, Pei ZJ, Treadwell C (2016) Rotary ultrasonic machining of CFRP: a comparison with grinding. Ultrasonics 66:125–132. https://doi.org/10.1016/j.ultras.2015.11.002

16. Moghaddas MA, Short MA, Wiley NR, Yi AY, Graff KF (2018) Improving productivity in an ultrasonic-assisted drilling vertical machining center. J Manuf Sci Eng 140(June):1–9. https://doi.org/10.1115/1.4039109

17. Azarhoushang B, Akbari J (2007) Ultrasonic-assisted drilling of Inconel 738-LC. Int J Mach Tools Manuf 47(7–8):1027–1033. https://doi.org/10.1016/j.ijmachtools.2006.10.007

18. Y. Li1, Y. Yang, Y (2022) Study on the simulation and experiment of ultrasonic-assisted vibration drilling of Ti6Al4V J Phys Conf Ser Pap 2242:1-8 https://doi.org/10.1088/1742-6596/2242/1/012011

19. Abdelkawy A, Hossam M, El-hofy H (2019) Mathematical model of thrust force for rotary ultrasonic drilling of brittle materials based on the ductile-to-brittle transition phenomenon. Int J Adv Manuf Technol 101:801–813

20. Liu Y, Pan Z, Li Q, Qi Z, Chen W (2022) "Experimental and scale - span numerical investigations in conventional and longitudinal torsional coupled rotary ultrasonic – assisted drilling of CFRPs." Int J Adv Manuf Technol 1707–1724. https://doi.org/10.1007/s00170-021-08286-7.

21. Baraheni M, Amini S (2019) Comprehensive optimization of process parameters in rotary ultrasonic drilling of CFRP aimed at minimizing delamination. Int J Light Mater Manuf. https://doi.org/10.1016/j.ijlmm.2019.03.003

22. Pei ZJ, Prabhakar D, Ferreira PM, Haselkorn M (1995) A mechanistic approach to the prediction of material removal rates in rotary ultrasonic machining. J Eng Ind 117(2):142. https://doi.org/10.1115/1.2803288

23. Liu D, Cong WL, Pei ZJ, Tang Y (2012) A cutting force model for rotary ultrasonic machining of brittle materials. Int J Mach Tools Manuf 52(1):77–84. https://doi.org/10.1016/j.ijmachtools.2011.09.006

24. Guba N, Schumski L, Paulsen T, Karpuschewski B (2022) Vibration-assisted deep hole drilling of the aluminum material AlMgSi0.5. CIRP J Manuf Sci Technol 36:57–66. https://doi.org/10.1016/j.cirpj.2021.11.002

25. Singh G, Jain V, Gupta D, Ghai A (2016) Optimization of process parameters for drilled hole quality characteristics during cortical bone drilling using Taguchi method. J Mech Behav Biomed Mater 62:355–365. https://doi.org/10.1016/j.jmbbm.2016.05.015

26. Ding K, Fu Y, Su H, Chen Y, Yu X, Ding G (2014) Experimental studies on drilling tool load and machining quality of C/SiC composites in rotary ultrasonic machining. J Mater Process Technol 214(12):2900–2907. https://doi.org/10.1016/j.jmatprotec.2014.06.015

27. K. Alam, A. V. Mitrofanov, and V. V. Silberschmidt, "Measurements of surface roughness in conventional and ultrasonically assisted bone drilling," Am J Biomed Sci. 312–320, 2009. https://doi.org/10.5099/aj090400312.

28. Jiao Y, Hu P, Pei Z J, Treadwell C (2005) Rotary ultrasonic machining of ceramics: design of experiments. Int J Manuf Technol Manag 7(2/3/4):192. https://doi.org/10.1504/IJMTM.2005.006830

29. Airao J, Nirala CK, Bertolini R, Krolczyk GM, Khanna N (2022) Tribology international sustainable cooling strategies to reduce tool wear, power consumption and surface roughness during ultrasonic assisted turning of Ti-6Al-4V. Tribol Int 169:107494. https://doi.org/10.1016/j.triboint.2022.107494

30. A. Abdelkawy and H. El, "Experimental and statistical study for measurements of surface roughness and hole geometry of ultrasonic - assisted drilling of soda glass." J. Brazilian Soc. Mech. Sci. Eng. 2021. 5. https://doi.org/10.1007/s40430-021-03172-5.

31. Abdelkawy A, Hossam M, El-hofy H (2019) Experimental investigation of the cutting forces and edge chipping in ultrasonic-assisted drilling of soda glass. pp 1433–1449

32. Rafik M, Mohamed N, Sharma S, Singh J (2020) Evaluation of surface roughness in the turning of mild steel under different cutting conditions using backpropagation neural network. Proc Est Acad Sci 69:109–115

33. Demuth H (2004) Neural network toolbox for use with MATLAB," The mathworks

34. Van Nguyen TH, Nguyen TT, Ji X, Do KTL, Guo M (2018) "Using artificial neural networks (ANN) for modeling predicting hardness change of wood during heat treatment using artificial neural networks (ANN) for modeling predicting hardness change of wood during heat treatment", IOP Conf. Ser Mater Sci Eng Pap 394:1–7. https://doi.org/10.1088/1757-899X/394/3/032044

35. Elsadek AA, Gaafer AM, Mohamed SSMAA (2020) Prediction and optimization of cutting temperature on hard - turning of AISI H13 hot work steel. SN Appl Sci 2(4):1–12. https://doi.org/10.1007/s42452-020-2303-5